Particle and wave dynamics in a magnetized plasma subject to high rf pressure

W. Gekelman and R. L. Stenzel

Department of Physics, University of California, Los Angeles, California 90024
(Received 28 June 1976; final manuscript received 21 April 1977)

The nonlinear response of a plasma subject to an intense, spatially localized rf field has been investigated experimentally. In a uniform quiescent magnetoplasma of density $n_e \gtrsim 10^9$ cm^{-3}, temperature $kT_e \simeq 5$ $kT_i \simeq 1$ eV, and magnetic field $B_0 \sim 100$ G, a resonance cone ($\omega/\omega_c \simeq 0.1$; where ω_c is the electron cyclotron frequency) is established which converges away from a circular exciter to reach a maximum amplitude at the remote cone apex. When an rf burst of intensity $\epsilon_0 E_{rf}^2/n_e kT_e \lesssim O(1)$ is applied, a strong density depression ($\delta n_e/n_e \simeq 40\%$) is formed in the focal region on a time scale (~ 1 μsec) short compared with a collision time. Fast ion bursts [$(1/2)\, mv_i^2 \simeq 35$ eV $\gtrsim 100$ kT_i], large amplitude ion acoustic waves, but negligible electron temperature increases are observed. Density and resonance cone field interact nonlinearly and in time develop a state of turbulence. Ion heating ($\Delta T_i/T_i \simeq 100$) dominates over electron heating ($\Delta T_e/T_e \sim 2$). The direct measurements of the particle distributions with probes and energy analyzers are supplemented by test wave techniques. Small amplitude ion acoustic, electron plasma, and Bernstein waves are propagated through the region of high rf intensity and the perturbed plasma properties are deduced from the test wave behavior. The observed nonlinear collisionless interactions between particles and intense rf field are qualitatively explained by a model involving the ponderomotive force on electrons and acceleration of ions by space charge fields.

I. INTRODUCTION

The behavior of a plasma in an intense high frequency field is of general interest in basic plasma physics and of particular importance in the fields of laser plasma interactions, rf heating, and space plasmas. The plasma response to an intense rf field is, in general, nonlinear, i.e., there is a self-consistent modification between the internal rf field and the plasma properties. In collisionless plasma, a nonuniform rf field exerts a time-average force, the ponderomotive force,[1] or radiation pressure[2] on the oscillating particles. The rf field is considered intense when the rf pressure is on the order of the thermal particle pressure. The particle dynamics are then governed by three forces: kinetic pressure, rf pressure, and magnetic field pressure.

We have experimentally investigated the nonlinear interaction between an intense localized rf field and a magnetized plasma. By means of a circular exciter structure, a resonance cone[3] is excited which converges away from the source. The maximum field is obtained at the remote cone apex. With this arrangement we can investigate the wave-plasma interaction free from undesirable boundary effects by the exciter or other structures. In a previous paper[4] we presented time and space resolved measurements of the rf field and the density profile when an intense ($\epsilon_0 E_{rf}^2/n_e kT_e \gtrsim 0.1$) rf burst ($\omega/\omega_c \gtrsim 0.1$, $\omega_c \simeq \frac{1}{4}\omega_p \simeq 2\pi \times 300$ MHz) was applied. A strong transient density depression ($\delta n_e/n_e \gtrsim 40\%$) was created in the region of highest rf intensity on a time scale short compared with a collision period. The density perturbation in turn modified the resonance cone pattern, and the nonlinear, nonstationary process evolved into a turbulent state.

In the present paper we investigate the particle dynamics in the nonlinear interaction. Time and space resolved Langmuir probe traces yield the electron distribution while similar measurements with gridded energy analyzers give the ion distribution. Special precaution is taken so that the probe data are not affected by the strong rf fields. Although the ions do not respond to the high frequency field ($\omega \gg \omega_{pi}$), we find their energy is dramatically enhanced whereas that of the oscillating electrons shows only a minor increase. For short rf pulses ($t_{rf} \simeq 2$ μsec), the ion distribution exhibits fast particle burst along $\mathbf{B}_0$ of directed energy $\frac{1}{2} m_i v_i^2 \gtrsim 35$ eV (unperturbed $kT_i \simeq 0.2$ eV); for long rf pulses ($t_{rf} \gtrsim 10$ μsec) when turbulence has developed isotropic ion heating to $kT_i \simeq 40$ eV and some electron heating ($\Delta T_e/T_e \simeq 2$) are observed. The presence of fast ions is verified independently by time-of-flight measurements of the associated density perturbations and by the damping effects on test ion acoustic waves. Likewise, the probe data for the electron temperature are supplemented by test wave diagnostics. Electrons plasma waves sensitive to the parallel electron temperatures $T_{e\parallel}$, and electron Bernstein waves sensitive to $T_{e\perp}$ indicate that no significant electron heating occurs.

The surprising result that a high frequency field, which in the linear regime interacts only with the electrons, leads, in the nonlinear regime, to strong ion heating is qualitatively explained by the following collisionless model: The intense nonuniform rf field exerts a ponderomotive force, $F \propto -\nabla \langle E_{rf}^2 \rangle$, on the electrons. The oscillating electrons drift out of the intense rf field region. The resulting space charge separation gives rise to a transient dc electric field which accelerates ions. Ions and electrons drift together, thereby approximately preserving charge neutrality. Due to the large mass difference, a drift velocity corresponding to a fraction of the electron thermal velocity results in ion velocity increases large compared with their initial thermal velocities. Thus, large ion perturbations and relatively small changes in the electron distribution can be expected.

 Copyright © 1977 American Institute of Physics

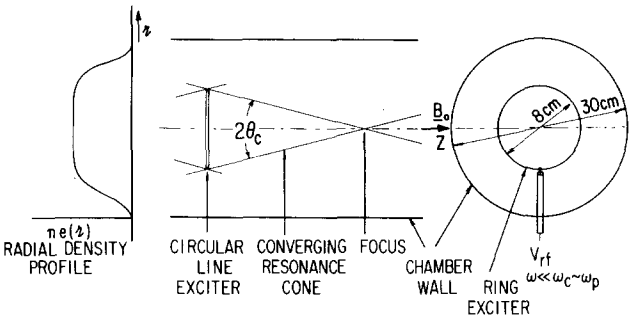

FIG. 1. Schematic view of the focused resonance cone setup.

The local particle drifts modify the density profile which in turn changes the resonance cone pattern. This nonlinear interaction described in more detail in Ref. 4 leads, in time, to a random growth and decay of many local density depressions and rf field enhancements. Random ion acceleration in space and time may then account for the hot, nearly Maxwellian ion distributions observed for long rf pulses.

The paper is divided into four sections. After briefly describing the experimental setup and measurement techniques in Sec. II, the measurement results are presented and discussed in Sec. III. The observations are summarized in Sec. IV and some conclusions on collisionless ion heating by nonuniform rf fields are drawn.

II. EXPERIMENTAL ARRANGEMENT

The experimental apparatus as well as several diagnostic techniques have been described in a previous publication.[5] Thus, only a brief description of the plasma and the experimental procedures will be given here emphasizing the particle diagnostic aspect.

The experiment is performed in a quiescent magnetized discharge plasma, uniform over approximately 14 cm diam and 180 cm length. The typical plasma parameters in the present experiment are: density $n_e \gtrsim 10^9$ cm^{-3}, temperature $kT_e \simeq 1$ eV, magnetic field $B_0 \simeq 125$ G, gas Xe, Ar at 2×10^{-4} Torr, low frequency fluctuations $\delta n_e/n_e \gtrsim 1\%$, collision frequency $\nu_{en}/\omega \simeq 10^{-3}$. The steady state plasma is diagnosed with small Langmuir probes, an X-band microwave interferometer, and test wave techniques. The absolute value of the plasma density is determined with cylindrical Langmuir probes and, more accurately, by measuring the resonance cone angle ($\omega \ll \omega_c \sim \omega_p$) in the linear regime.[3]

A pulsed rf signal ($\omega/2\pi \simeq 50$ MHz, $P_{rf} \lesssim 25$ W, $t \lesssim 5$ μsec, $t_r \simeq 1$ msec) is applied to a circular (8 cm diam) exciter structure located on the axis of the plasma column in a plane perpendicular to $\mathbf{B}_0$ (see Fig. 1). The rf potential distribution and electric field are measured with a differential T probe consisting of two field-aligned parallel wires (1 cm long, 0.1 mm diam, 3 mm spacing), connected via miniature coaxial cables (1 mm o.d.) to a balanced transformer.[4]

The ion velocity distribution is measured with a miniature retarding grid velocity analyzer which provides radial and angular spatial resolution. The casing is constructed of glass with outer diameter of 3 mm. The grid and collector diameters are 1 mm. These dimensions are small compared with an ion Larmor radius. The device has an energy resolution of $\gtrsim 1$ eV. Larger analyzers with better resolution were seen to seriously disrupt the rf pattern and attendant phenomena.

Since in this experiment we wished to observe the evolution of nonlinear phenomena, repetitive rf bursts were applied and the effects analyzed using sample-and-hold techniques. Besides the temporal resolution, our probe arrangement provided two-dimensional spatial resolutions along and across $\mathbf{B}_0$.

III. EXPERIMENTAL RESULTS

Since the aim of this work is to study the particle dynamics in a region of intense rf pressure, we will briefly review how this region is produced and what the previously observed nonlinear effects are.

A. Rf field and density profiles

A circular antenna shown in Fig. 1 gives rise to a converging resonance cone in the quasi-electrostatic near-zone of the radiation pattern. In the cold plasma limit, the cone angle θ_c is a function of applied frequency ω, electron plasma frequency ω_p, and electron cyclotron frequency ω_c, given by

$$\theta_c = \sin^{-1}\left\{\left(\frac{\omega}{\omega_c}\right)^2\left[1+\left(\frac{\omega_c}{\omega_p}\right)^2-\left(\frac{\omega}{\omega_p}\right)^2\right]\right\}^{1/2}, \qquad (1)$$

where $\omega < \min(\omega_p, \omega_c)$. Figure 2(a) shows the observed rf pattern in the linear regime. Contours of constant relative rf potential are displayed on the r, z plane which represents a cut through the cone along its axis parallel to $\mathbf{B}_0$. The feeding transmission line to the ring exciter is normal to the plane of measurement. Since the loop is small compared with the free space wavelength and is made of a good conductor, the applied signal is constant around the loop. Thus, the radiation pattern should be azimuthally symmetric. The exciter, 8 cm diam, is located at $z = 0$, approximately 36 cm to the left of the focus. The cone trajectory is indicated by dashed lines through the radial field maxima (triangular data points). In the narrow focal region (< 1 cm diam, ~4 cm length) the rf amplitude is approximately an order of magnitude larger than near the exciter.

When the input voltage to the exciter is increased, the rf field in the plasma becomes nonlinear and changes its pattern in time. Figure 2(b) displays the rf pattern 5 μsec after the turn-on of an rf burst 43 dB larger than that in Fig. 2(a). One can see that the focal region has been considerably widened. The cone on the exciter side of the focal region is distorted while the outgoing cone structure is destroyed. The rf pattern begins to change randomly in space and time. During the high power burst, there is a transition in time from a sharply focused pattern as in Fig. 2(a) to one such as in Fig. 2(b). The time scale for the nonlinear modification depends upon the applied rf intensity and is typically a few μsec for $\epsilon_0 E_{rf}^2/n_e kT_e \simeq 0.1$. For very long rf bursts, characteristic of steady-state conditions, the rf field spreads

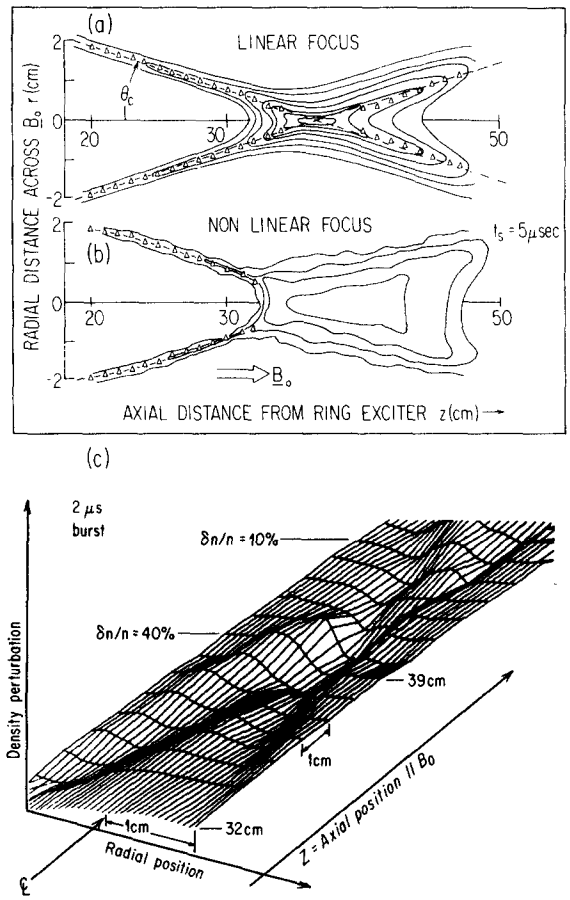

FIG. 2. Contour maps of rf field and density in the r-z plane parallel to the cone axis near the focus. (a) Contours of constant relative rf field in the linear regime (center 100%, each contour 15% decrease). Parameters: $\omega/2\pi = 50$ MHz, $\omega/\omega_c = 0.081$, $\omega_p/\omega_c = 1.9$, $V_{rf} = 0.35\ V_{rms}$. (b) Contour map of the nonlinear resonance cone field sampled at $t_s = 5$ μsec after the turn-on of an rf burst of $V_{rf} = 17.5\ V_{rms}$. Frequency parameters as in (a). (c) Three-dimensional view of the density perturbation determined from the electron saturation current, sampled at $t_s = 0.5$ μsec after the end of a 2 μsec long intense rf burst of parameters as in (b).

out over most of the plasma column such that the cone structure is lost. The rf amplitude is lower on the average, but exhibits local maxima and minima distributed randomly.

The modification of the rf pattern correlates with changes in local plasma density. Figure 2(c) is a computer drawn, three-dimensional display of the measured density profile sample 0.5 μsec after a 2 μsec long burst. One sees that a large density depression ($\delta n_e/n_e \simeq 40\%$) exists at the focus; the perturbation follows the cone trajectory and decreases at increasing distance from the focus. For longer rf bursts or higher rf intensities, the density depression splits into multiple peaks and valleys and eventually develops a turbulent pattern analogous to the random behavior of the rf pattern. The turbulence is observed on oscilloscope traces since sampling techniques average random fluctuations out to zero. It was previously observed that after the rf was switched off the density perturbation relaxed in the direction perpendicular to the magnetic field by moving outward at approximately sound speed.

In this paper we wish to address ourselves to the particle dynamics and develop a picture of the formation of this cavity and its subsequent breakup.

B. Ion dynamics

Since a substantial fraction of the plasma is expelled from the focal region on a time scale short compared with the propagation of an ion acoustic wave across it, one would expect to see appreciable ion acceleration. The flow should be dominantly along the magnetic field because the electrons are strongly magnetized. We have therefore measured the ion distribution with a miniature velocity analyzer positioned on the column axis at $\Delta z = 2.5$ cm beyond the focus which in turn is 41.5 cm away from the loop exciter. The analyzer collector is facing toward the focus. All measurements are taken after the end of the rf burst since the presence of strong rf fields makes probe measurements impossible. Figure 3(a) shows the collector current versus retarding grid potential sampled at fixed times t_s after the end of a 2 μsec long intense rf burst. At long times after the burst ($t_s \gtrsim 40$ μsec), the trace is identical to that in the unperturbed state where the ion temperature is approximately $kT_i \simeq 0.2$ eV. At 1 μsec after the burst, the current is appreciably larger than in the unperturbed state, and continues to increase for two microseconds. It will be shown that this flux increase is due to a burst of fast particles arriving at the detector. The time-of-flight indicates velocities of approximately $v = 6\times10^5$ cm/sec

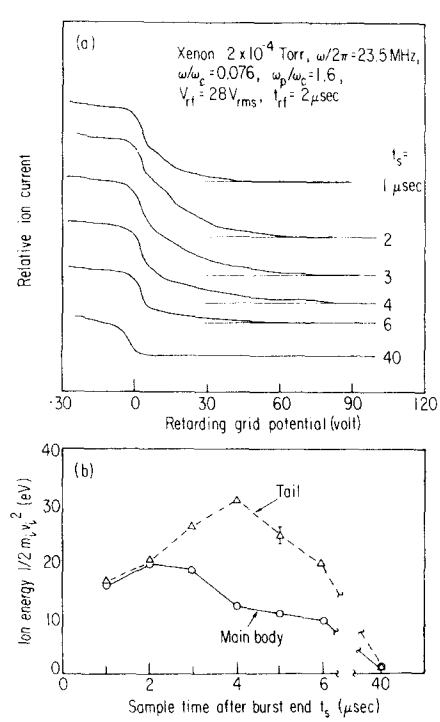

FIG. 3. (a) Sampled ion velocity analyzer traces at different times t_s after the end of an intense rf burst. (b) Average energies in the body and tail of the ion distribution function vs time t_s. The delay in the arrival of fast ions is due to propagation from the focal region to the analyzer ($\Delta z = 2$ cm).

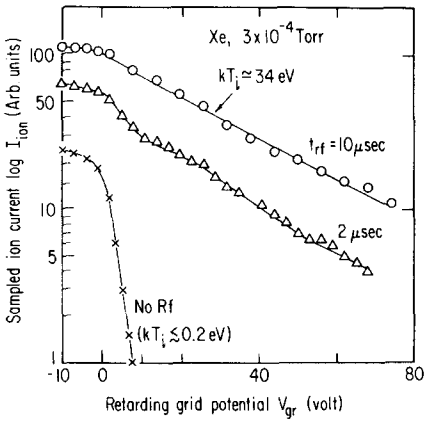

FIG. 4. Ion velocity analyzer traces sampled at $t_s = 3$ μsec after the end of rf bursts of different lengths t_{rf}. For long rf bursts a hot Maxwellian ion distribution is observed. Parameters: $\omega/2\pi = 23.5$ MHz, $\omega/\omega_c = 0.076$, $\omega_p/\omega_c = 1.6$, $V_{rf} = 28$ V_{rms}.

which is seven times larger than sound speed in the xenon discharge with $kT_e \simeq 1$ eV ($C_s \simeq 0.84 \times 10^5$ cm/sec). As time goes on, the flux to the velocity analyzer decreases because the particle burst propagates outward and leaves a density depression behind. For short rf bursts, the perturbed ion distribution function can be characterized by a main body with an energetic tail, both of which have mean energies larger than the unperturbed ion temperature ($kT_i \simeq 0.2$ eV). The temporal evolution of the effective ion "temperatures" is illustrated in Fig. 3(b).

When the velocity analyzer is rotated by 90° so as to measure the perpendicular ion velocity distribution, the behavior is similar to Fig. 3, but the magnitude of the energetic particle flux is decreased, For a rotation by 180° when the analyzer faces away from the focal region, only very small tails are observed. Radial velocity analyzer scans indicate a maximum of the fast ion production in the column center and essentially no fast ions near the column edge. Thus, the energetic ions mainly originate from the focal region and move out along B_0 with some perpendicular spread. Here, it should be emphasized again that there are no exciter structures, boundaries, plasma nonuniformities, etc. in or near the intense rf region and that the ion acceleration can only be the result of the strong rf field.

The simple density depression shown in Fig. 2(c) is only the first phase of a nonstationary process. When the rf is applied for longer times, the density depression is observed to split up into two and then several minima with adjacent maxima, and finally into a randomly distributed turbulent-like density pattern. The corresponding evolution of the ion distribution function is shown in Fig. 4 which displays the sampled collector current on a logarithmic scale vs retarding voltage for different rf bursts lengths. Again, the traces are sampled 1 μsec *after* the end of the rf burst. For the 2 μsec rf pulse, we can distinguish several high energy tails due to fast ion bursts of different energies; but, for a 10 μsec rf pulse, the energetic tails have merged to a nearly Maxwellian distribution whose temperature is more than 100 times larger than the initial ion temperature. We also note that the ion saturation flux, $j_+ = n_e e[k(T_e + T_i)/m_i]^{1/2}$, has increased by a factor of about 5 consistent with the observed ion heating to $kT_i \simeq 34\ kT_e$ and an average density decrease $\delta n_e/n_e \simeq 10\%$. It will be shown that the electron temperature increase is relatively small ($\Delta T_e/T_e \simeq 2$) and can therefore not account for the ion flux increase.

From the spatial resolution of the analyzer, the non-Maxwellian tails for short rf pulses have been tentatively identified as fast ion bursts streaming away from the focal region. For long rf pulses, the ion distribution is observed to be nearly independent of direction and radial position. Thus, one may suspect that the isotropic hot ion distribution is the result of multiple ion accelerations due to the random formation of density depressions over a wide spatial region.

The growth and propagation of the fast ion bursts has been investigated by taking time-resolved two-dimensional density maps. The density is derived from the electron saturation current to a small disk Langmuir probe (2 mm diam) sampled after the end of the rf pulse. Figure 5 gives examples of density perturbation maps sampled at different times. Since sampled data are averaged over many pulses, the large fluctuations around the averages are lost in this display. Contours of density maxima (heavy lines) and density minima (thin lines) are shown in a plane cut along the cone axis near the focal region which is 23 cm axially away from the exciter. Comparison between Figs. 5(a) and (b) shows that the density compressions and rarefactions move away from the regions of highest rf intensities. For example, the perturbation labeled A becomes deformed during the 2

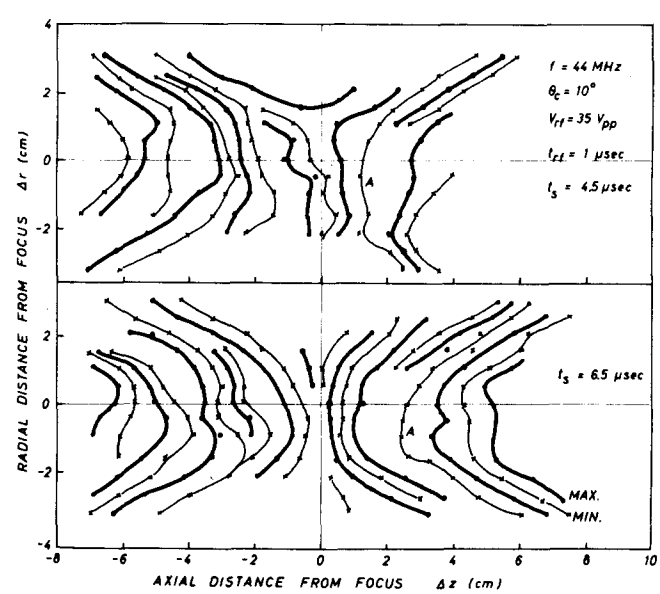

FIG. 5. Maps of the density perturbations in the r-z plane around the focal region (note scale differences). The contours of the density maxima (heavy lines) and minima are sampled at two different times ($t_s = 4.5$, 6.5 μsec) after the end of a 1 μsec long rf pulse. Propagation effects indicate source and speed of the fast ion bursts. Parameters: $\omega/2\pi = 44$ MHz, $\omega/\omega_c = 0.14$, $\omega_p/\omega_c \simeq 1.6$, $V_{rf} = 12.4\ V_{rms}$, argon 2×10^{-4} Torr.

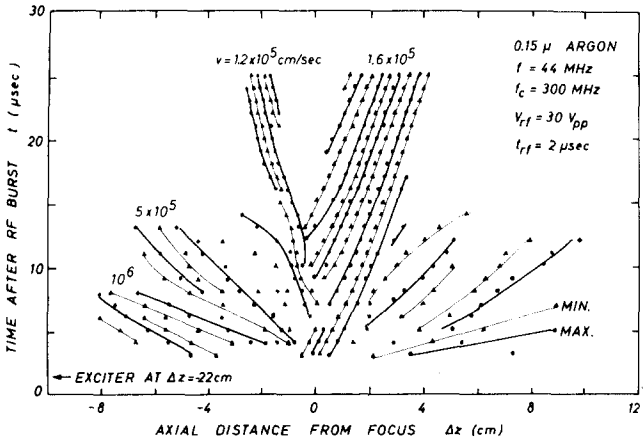

FIG. 6. Arrival time of density perturbations after the rf burst end vs axial position ($r=0$). This time-of-flight diagram indicates the generation of fast ion bursts ($v_i \gg C_s$) and ion acoustic waves ($v \simeq C_s$) due to the impact of high rf pressure in the focal region. Parameters: $\omega/2\pi = 44$ MHz, $\omega/\omega_c = 0.14$, $\omega_p/\omega_c \simeq 1.6$, $V_{rf} \approx 11$ V_{rms}, $t_{rf} = 2$ μsec, argon 1.5×10^{-4} Torr.

μsec time interval, but as a whole it translates to the right. The deformation indicates velocity spread which results from spatial variations in the ponderomotive force. The major component of its velocity is axial and is approximately 8×10^5 cm/sec or five times the unperturbed sound speed ($C_s \simeq 1.5\times10^5$ cm/sec in argon at $kT_e \simeq 1$ eV). Such fast moving large amplitude perturbations are not ion acoustic wave phenomena but clumps of fast moving ions. Time-of-flight measurements show that the propagation speed is consistent with the ion energies from the velocity analyzer traces.

An example of such time-of-flight measurements is shown in Fig. 6. It shows the position along the cone axis of density maxima and minima vs time after the end of the rf pulse. One can distinguish two characteristic perturbations. At early times the trajectories of small slope indicate bursts of fast particles which shoot axially out of the focal region with velocities up to $v \simeq 10^6$ cm/sec $\simeq 7\ C_s$. At larger time ($t \gtrsim 10$ μsec) an ion acoustic wave packet emerges from the focal region as indicated by the

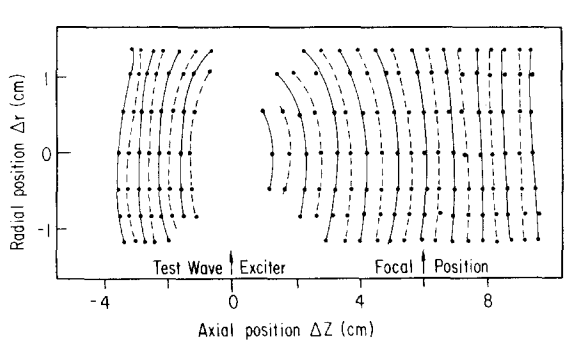

FIG. 7. Phase contours of ion acoustic test waves launched with a small wire probe in a uniform magnetoplasma (note different scales in r and z direction). By placing the exciter at $\Delta z \simeq 6$ cm from the focal region, a nearly perfect test wave propagating along B_0 can be generated in the focus. Parameters: $f_1 = 230$ kHz, $n_e = 4.7\times10^9$ cm^{-3}, $kT_e \simeq 1$ eV, $B_0 = 118$ G, argon 1.5×10^{-4} Torr.

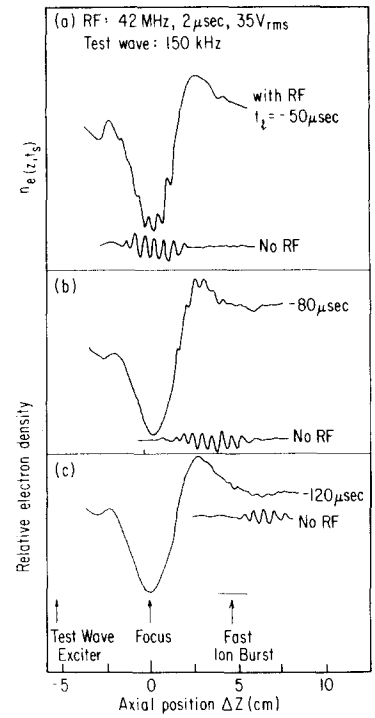

FIG. 8. Test ion acoustic waves propagating through the perturbed plasma. The traces are sampled at $t_s = 2$ μsec after the end of an intense rf burst. The ion wave packet is launched at different times t_i prior to the rf burst so as to position it at different locations with respect to the focus. For reference, the test wave in the absence of the strong rf pulse is indicated. Strong test wave damping is observed in regions of the fast ion bursts. Parameters: $\omega/2\pi = 42$ MHz, $\omega/\omega_c = 0.14$, $\omega_p/\omega_c = 1.9$, $V_{rf} = 35$ V_{rms}, $t_{rf} = 2$ μsec, xenon 7×10^{-5} Torr.

steeper trajectories. The propagation speed is within 10% of the sound speed. A small axial drift ($v_d/C_s \simeq 0.1$) in the z direction is responsible for an axial asymmetry in propagation speed and damping. It is assumed that the acoustic perturbation is generated in the recovery process of the density cavity at the cone focus.

A further independent diagnostic of the ion distribution employs the propagation of test ion acoustic waves. A small wire (3 cm length, 0.25 mm diam) aligned perpendicular to B_0 is used to excite small amplitude ion acoustic waves. The phase fronts for a tone burst 12 cycles long propagating in a quiescent argon plasma are shown in Fig. 7. They are curved near the exciter, but several centimeters away one has nearly plane waves. By placing the exciter about 5 cm from the focal region, which avoids interference with the resonance cone pattern, we can excite a clean ion acoustic wave packet in the focal region. Since in xenon (Fig. 8) the ion acoustic speed is relatively small ($C_s \simeq 1.3$ mm/μsec), the test wave is launched 50 μsec or more before the rf burst is turned on. Heavy ion gases are preferred in these experiments since the time scale for the perturbation is long. By adjusting the launch time, t_i, the ion acoustic wave packet may be positioned at any desired point in the focal region.

Figure 8 illustrates a test wave placed at several different positions. In each case the lower trace indicates

the axial position of the ion wave when no burst was present. Figure 8(a) finds the wave in the center of the density cavity. It is not severely affected; its speed and amplitude are unchanged although a phase change is present. There is a significant change in the wave damping, however, when the wave is placed near the shoulder of the perturbation. In Fig. 8(b) the test wave straddles the edge of the density perturbation. Strong damping is observed on the crest which is the region of the outward moving fast ions. In Fig. 8(c), the test wave is completely damped. Note that these changes occur within about one ion period since the rf burst is shorter than the ion wave period.

The collisionless damping rate of ion acoustic waves is sensitive to the ratio of the electron-to-ion temperature. In the next part, we will show that the electron temperature remains relatively unchanged. One may therefore interpret the observed strong damping by ion heating to at least such levels that there are large numbers of particles at sound speed present in the distribution ($kT_i > kT_e$). The strong damping also excludes the generation of mono-energetic beams. Although the fast ions have a preferred flow direction, there must be a significant energy spread and a decreasing number of particles with increasing energy. These observations qualitatively confirm the velocity analyzer and time-of-flight measurements.

C. Electron dynamics

Since the applied frequency ($f \simeq 50$ MHz) is well above the ion plasma frequency ($f_{pi} < 2$ MHz) and the resonance cone is only due to the collective electron response, one might expect a severe perturbation of the electron distribution function after an intense rf burst. The peak rf field strength is approximately[4] $|E_{rf}|_{max} \simeq 100$ V/cm such that $\epsilon_0 E_{rf}^2/n_e kT_e \gtrsim 1$. The surprising result is that virtually no electron heating is observed.

The electron distribution has first been measured with Langmuir probes. These measurements are again restricted to sampling times after the end of the rf burst. During the intense rf field, electrons gain oscillatory velocities comparable to their thermal velocities and the resulting non-Maxwellian distribution function makes conventional probe theories inapplicable. The observed probe traces during the rf pulse are strongly modified and take approximately 500 nsec to recover. This effect is illustrated in Fig. 9. For reference, the rf pattern and various probe positions (A to E) are indicated on the top. Two Langmuir traces sampled during the rf burst are shown at the bottom, one in the rf focus (B) and the second one on the same flux tube but outside of the rf region (E). It is quite obvious that the wide retardation region in trace B compared with that of trace E cannot be due to genuine heating because a steep temperature gradient along the magnetic field cannot be maintained over a distance short compared with the mean free path. We also note that the electron saturation current does not increase proportional to $T_e^{1/2}$, and the discrepancy cannot be accounted for by a density decrease. The apparent "temperatures" from similar traces at other points summarized on the right side of Fig. 9 indicate the correla-

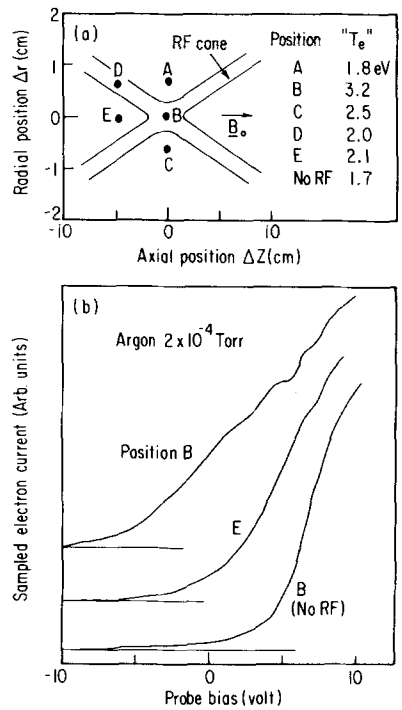

FIG. 9. (a) Schematic drawing of resonance cone and location of Langmuir probe. The apparent temperature T_e at these locations are indicated on the right. (b) Langmuir probe traces sampled during an intense rf burst (3 μsec after turn-on) at different positions. Trace B reflects rf perturbations on the probe rather than true heating. Horizontal lines indicate current zero level. Parameters: $\omega/2\pi = 50$ MHz, $\omega/\omega_c = 0.105$, $\omega_p/\omega_c \simeq 9$, $V_{rf} \simeq 28\ V_{rms}$, argon 2×10^{-4} Torr.

tion between high T_e values and large rf amplitudes. The anomalously high temperature values disappear within 500 nsec to 1 μsec after the end of the rf pulse, at which time the temperature is uniform and, to within measurement accuracy, unchanged from the initial value. This time interval is short compared with the electron temperature decay time ($\tau_e \gtrsim 500$ μsec) which has previously been measured in a pulsed afterglow plasma.[5] Thus, if the electrons had been heated in the 3 μsec long intense rf burst, the energy relaxation should have been observable.

In addition to the probe diagnostics, we have used test waves to infer the particle dynamics. First, Langmuir waves are propagated along B_0 so as to obtain an independent check on the parallel electron temperature. The modes observed have a lower cutoff frequency and satisfy $k_{\parallel}a \gg 1$ where a is the column radius, thus are warm unbounded plasma modes rather than finite column modes. From the Bohm–Gross dispersion, the relation between wavelength and temperature is given by

$$\lambda_{\parallel} = \left(\frac{3kT_e}{m_e}\right)^{1/2} \frac{2\pi}{(\omega^2 - \omega_p^2)^{1/2}} \quad . \tag{2}$$

The waves are launched from a straight wire (3 cm long, 0.13 mm diam) aligned perpendicular to B_0 and positioned away from the focal region so as not to interfere with the cone structure. The test wave frequency (350 MHz) is just above the electron plasma frequency ($f_p \simeq 346$ MHz) and much larger than the resonance cone frequency

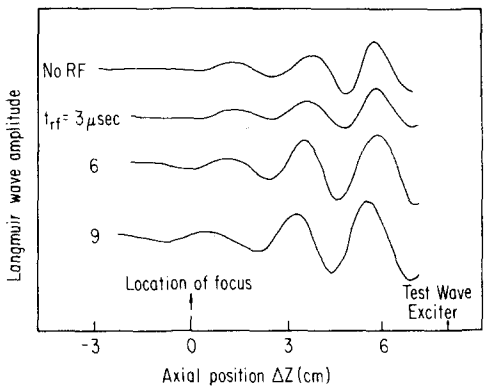

FIG. 10. Small amplitude test Langmuir waves sampled 2 μsec after intense rf bursts of different lengths t_{rf}. The test wave exciter is positioned on axis approximately 8 cm from the focus The focal region has an axial extent of approximately 3 cm. Wavelength changes indicate small electron heating. Parameters: $\omega/2\pi = 35$ MHz, $\omega/\omega_c = 0.125$, $\omega_p/\omega_c = 1.24$, $V_{rf} = 21\ V_{rms}$, $\omega_L/2\pi = 350$ MHz, argon 3×10^{-4} Torr.

(35 MHz). Wave propagation along B_0 and dispersion according to Eq. (2) have been verified.

Figure 10 shows interferometer traces of the test Langmuir wave sampled 2 μsec after the end of intense rf bursts of different lengths. The traces are taken along the cone axis but at a distance of several cm from the focus. The objective of this arrangement is to separate the effects of density and temperature perturbations on the wave dispersion. If electron heating occurred, the temperature increase would spread out along B_0 much faster than the density perturbations. For rf burst lengths below 3 μsec, no wavelength changes are observed well outside the focal region. Although such bursts create peak density perturbations of 40% at the focus, one cannot see Langmuir waves shortened to the expected wavelength of 0.45 cm in that region. The density cavity is surrounded by a density enhancement due to the expelled particles (see Fig. 8), which partially cuts off (that is attenuates) an incoming Langmuir wave. Since the rapid density variation $(n/\nabla n) \approx \lambda$ in focal region complicates the interpretation of the Langmuir waves only the region well outside the focus is used for diagnostic purposes. For long rf bursts ($t_{rf} = 9$ μsec) a wavelength increase of 30% is measured outside of the focal region from which a temperature change from $T_e \simeq 1$ eV to $T_e \simeq 1.7$ eV is inferred. Since the burst length is comparable to a collision period, the temperature increase may be due to collisional heating.

The second wave diagnostics involves Bernstein waves which propagate across the magnetic field and whose wavelength depends on the perpendicular electron temperature ($\lambda_\perp \propto T_{e\perp}^{1/2}$). Since the perpendicular wavelengths are small ($\lambda_\perp \sim 1$ mm), good spatial resolution is obtained. The waves are excited with a coaxially-fed T probe (4 cm long, 0.13 mm diam) aligned parallel to B_0 and positioned 1.5 cm radially displaced from the focal region, as shown in Fig. 11. This position corresponds to the edge of the density depression at 3.5 μsec after the end of the rf burst.

Since the Bernstein wavelengths depend on temperature and density, we have first singled out the density dependence. In a uniform plasma, the wavelength is measured as a function of density at constant ω, ω_c, kT_e. The measured dependence is consistent with the linear dispersion properties of Bernstein waves.[6,7]

After the end of an intense, but short rf burst ($t_{rf} = 2$ μsec), the radial Bernstein wave interferometer trace is sampled [see Fig. 11(a) top] and the local change in wavelength with respect to the unperturbed trace is noted. The evaluation of the perturbed interferometer traces is shown in Fig. 11(b) where the phase difference $\Delta\phi = \Delta kr$ between the perturbed and quiescent test wave is plotted vs radial position. $\Delta\phi$ is the local wavenumber difference normalized to 2π. From the unperturbed dispersion data, phase shifts of $\Delta\phi = 100°$ are found to correspond to density depressions of $\delta n_e/n_e \simeq 60\%$. One can see that the phase perturbation reflects the shape of the density perturbation previously measured with probes [see Figs. 2(c) and 8]. Thus, we do not find a perpendicular electron temperature increase as a result of the short, intense rf burst.

As previously noted from the Langmuir test waves, the electron temperature does increase for long rf bursts. Since the heating process is presumably collisional, i.e., isotropic, one may expect to also see perpendicular wavelength changes of test Bernstein waves. This effect is shown in Fig. 12. The sampling time of the test wave interferometer traces is kept fixed at 1 μsec after the end of the intense burst whose length is varied. We note that for the burst lengths $t_{rf} = 4$ μsec, the wavelength near the focus increases from $\lambda_\perp = 1.9$ mm ($t_{rf} = 0$) to a maximum of $\lambda_\perp \simeq 3$ mm. Before interpreting this effect as being due to an increase in $T_{e\perp}$, we have to subtract the

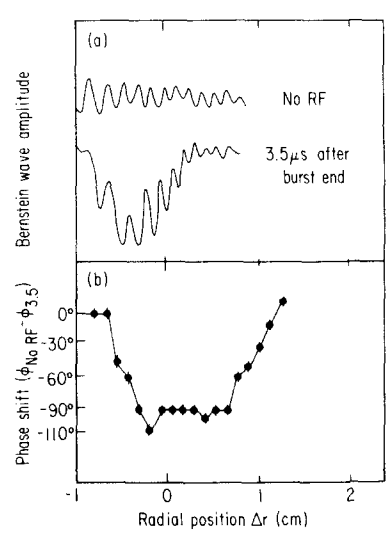

FIG. 11. (a) Small amplitude Bernstein waves sampled without rf and 3.5 μsec after a 2 μsec long rf burst focused radially at $r \simeq 0$. The test wave exciter is located radially at $\Delta r = -1$ cm and axially at the focal position. (b) The phase change of the test waves displayed in (a) Vs radial position reflects the density cavity shape. Phase changes indicate $\delta n_e/n_e \simeq -40\%$. Parameters: $\omega/2\pi = 37.5$ MHz, $\omega_B/2\pi = 315$ MHz, $V_{rf} = 2$ μsec, $\omega_p/\omega_c = 1.4$, $\omega_B/\omega_c = 1.13$, argon 2×10^{-4} Torr.

effects of the density decrease. For long rf bursts the density fluctuates randomly and the perturbations are, in general, smaller ($\delta n_e/n_e \gtrsim 20\%$) than in the initial formation of the single depression. Thus, from the 60% wavelength increase, at most 20% may be accounted for by the density decrease. The remaining wavelength increase by a factor of 1.4 may then be explained by a tem perature increase by a factor $T_{\perp f}/T_{\perp i} = 1.96$, where $T_{\perp f}$, $T_{\perp i}$ are final and initial perpendicular electron temperatures. This value is in reasonable agreement with the results from the Langmuir test waves.

Finally, we have propagated test Bernstein waves during and just after the end of a short ($t_{rf} = 2$ μsec) intense rf burst which, as previously shown, causes no heating. Typical sampled interferometer traces are shown in Fig. 13. During and just after the end of the rf burst, strong test wave damping is observed. After about 1 μsec the test wave trace has essentially recovered to the unperturbed shape. Due to the short rf burst length, density turbulence cannot account for the strong damping effect. The strong damping is obviously a result of the modified electron distribution function. When the electrons acquire oscillatory velocities on the other of their thermal velocity, strong mode coupling effects occur. The test wave energy may then be rapidly transferred into multiple sidebands ($\omega = \omega_B \pm n\,\omega_{rf}$, $n = 1, 2, \ldots,$ where ω_B is the test Bernstein wave frequency) which are not detected in an interferometer setup. The present simple test wave diagnostics is therefore restricted from the time interval of the rf burst and from the recovery period ($t_r \lesssim 1$ μsec) during which the perturbed distribution function relaxes to a Maxwellian. It is interesting to note that the perturbed Langmuir probe and velocity analyzer traces recover with the same time constant, hence the reason for the anomalous traces is also presumably the large oscillatory electron motion.

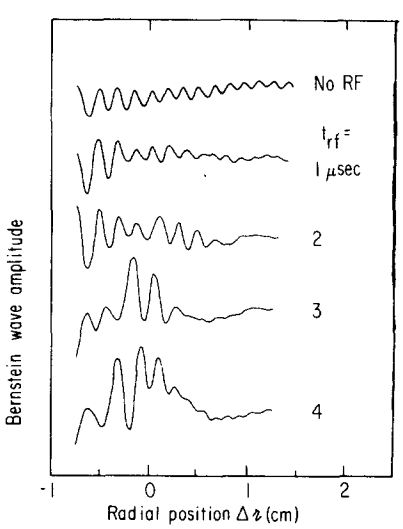

FIG. 12. Small amplitude Bernstein waves in focal region sampled 1 μsec after intense rf bursts ($V_{rf} = 24.8$ V_{rms}) of varying lengths t_{rf}. Increased wavelengths are partly due to electron heating and partly due to density decrease. Rf focal position is at $r = 0$. Parameters: $\omega/2\pi = 37.5$ MHz, $\omega/\omega_c = 0.12$, $\omega_p/\omega_c = 1.45$, $\omega_B/\omega_c = 1.13$, argon 4×10^{-4} Torr.

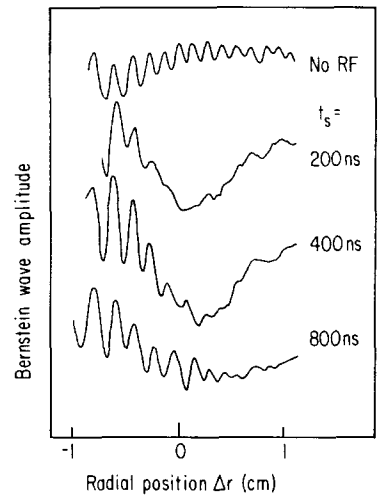

FIG. 13. Small amplitude Bernstein waves sampled at early times after an intense rf burst. The test waves are launched from radial position $\Delta r = -1$. The rf is focused at $\Delta r \simeq 0$. t_s is the sample time after the end of a 2 μsec duration burst. Strong wave damping is observed in the focal region for t_s < 500 nsec. Plasma parameters: $\omega/2\pi = 37.5$ MHz, $\omega_B/\omega = 8.4$, $V_{rf} = 24.8$ V_{rms}, $\omega_p/\omega_c = 1.40$, $\omega_B/\omega_c = 1.13$, argon 2×10^{-4} Torr.

IV. SUMMARY AND CONCLUSIONS

The present experiment is an extension of our previous investigation[4] of the nonlinear interaction of an intense localized rf field with a plasma. Here, we have studied the particle dynamics using probe and wave diagnostic tools. The main result is the observation of strong ion acceleration and heating yet negligible collisionless electron heating. These observations support our previous physical picture of the interaction whereby the ponderomotive force on the electrons gives rise to space charge fields which accelerate the ions. Ion heating is the result of random acceleration in a turbulent rf pattern which evolves from the nonlinear interaction between the resonance cone and the plasma density.

Since the experiment involves highly nonlinear plasma processes, great care was taken in the layout and diagnostics. In an initially uniform quiescent plasma, a localized rf field was produced free of boundary effects. The nonlinear evolution of the rf field, plasma density, and particle distributions were diagnosed with various tools providing temporal and spatial resolution. The nonlinear effects were observed on a time scale short compared with a collision period. Because of these various important aspects in a nonlinear wave experiment, we may make some remarks concerning pervious rf heating experiments. For example, in experiments on parametric instabilities near the lower hybrid frequency,[8] strong electron and ion heating has been observed. Since the exciter structures used in these experiments also give rise to nonuniform rf fields, the ion heating may be the result of the nonlinear interaction near the lower hybrid cones rather than due to wave-particle scattering associated with the decay instability.

Fast ion production in intense localized rf fields has also been observed in attempts to heat tokamak plasmas

near the lower hybrid frequency,[9] and in many laser plasma experiments.[10] However, these experiments cannot be diagnosed in detail, and the physics has to be investigated in scaled experiments.[11] The present experiment demonstrated in detail how an intense localized rf field causes ion heating. This experiment also suggests that highly nonuniform intense rf fields in the plasma interior could offer a new approach for strong ion heating with an external rf source.

ACKNOWLEDGMENTS

The authors gratefully acknowledge valuable discussions with Dr. G. Morales, Dr. Y. C. Lee, and Dr. A. Y. Wong.

This work was supported by the U. S. Energy Research and Development Administration under Grant No. AT(04-3)-34 PA 157.

[1]G. Schmidt, *The Physics of High Temperature Plasma, an Introduction* (Academic, New York, 1966), p. 47; H. Hora, in *Laser Interaction and Related Plasma Phenomena*, edited by H. J. Schwarz and H. Hora (Plenum, New York, 1971), p. 383.

[2]L. D. Landau and E. N. Lifshitz, *Electrodynamics of Continuous Media* (Pergamon, Oxford, 1966), pp. 67, 142, 242.

[3]H. H. Kuehl, Phys. Fluids **5**, 1095 (1962); R. K. Fisher and R. W. Gould, *ibid.* **14**, 857 (1971).

[4]R. Stenzel and W. Gekelman, Phys. Fluids **20**, 108 (1977).

[5]W. Gekelman and R. L. Stenzel, Rev. Sci. Instrum. **46**, 1386 (1975).

[6]I. B. Bernstein, Phys. Rev. **109**, 10 (1958).

[7]T. H. Stix, *The Theory of Plasma Waves* (McGraw-Hill, New York, 1962).

[8]R. P. H. Chang and M. Porkolab, Phys. Rev. Lett. **31**, 1241 (1973); and **32**, 1227 (1974).

[9]W. M. Hooke, Bull. Am. Phys. Soc. **20**, 1313 (1975).

[10]G. H. McCall, F. Young, A. W. Ehlers, J. F. Kephart, and R. P. Godwin, Phys. Rev. Lett. **30**, 1116 (1973).

[11]A. Y. Wong and R. L. Stenzel, Phys. Rev. Lett. **34**, 727 (1975).